Photochemical & Photobiological Sciences

RSC Publishing

PAPER

View Article Online
View Journal | View Issue

Photophysical properties of 3-[2-(*N*-phenylcarbazolyl)-benzoxazol-5-yl]alanine derivatives – experimental and theoretical studies†

Cite this: *Photochem. Photobiol. Sci.*, 2013, **12**, 284

Katarzyna Guzow,*[a] Marlena Czerwińska,[a] Agnieszka Ceszlak,[a] Marta Kozarzewska,[a] Mariusz Szabelski,‡[b] Cezary Czaplewski,[a] Anna Łukaszewicz,[b] Aleksander A. Kubicki[b] and Wiesław Wiczk[a]

Solvatochromic probes are often used in biophysical studies to obtain information about polarity of the microenvironment. As there is not much natural fluorophores with such properties, there is still need for new synthetic compounds such as 3-(2-benzoxazol-5-yl)alanine derivatives. Among this group of non-proteinogenic fluorescent amino acids especially interesting are 3-[2-(4-aminophenyl)benzoxazol-5-yl]-alanine derivatives whose solvatochromism depends on the substituents on the nitrogen atom, as revealed by our recent studies. To expand them we synthesized two new derivatives with an *N*-phenylcarbazole moiety in position 2 of the benzoxazole ring and studied their photophysical properties in solvents of different polarity and ability to form hydrogen bonds using absorption and steady-state and time-resolved fluorescence spectroscopy. Applying single parameter and multi-linear correlations with different solvent parameters, the excited state dipole moments were determined as well as the influence of solvent parameters on each photophysical property was estimated. Moreover, the geometry of compounds and vertical absorption transition were theoretically calculated (DFT and TD DFT methods). It was found that the place of substitution of the *N*-phenylcarbazole part by the benzoxazole unit determines the character of the electron transition (π–π* or ICT) and thereby the spectral and photophysical properties of the compounds studied.

Received 23rd April 2012,
Accepted 3rd September 2012

DOI: 10.1039/c2pp25114k

www.rsc.org/pps

1 Introduction

The solvatochromic effect is frequently used in biophysical studies of the polarity of the microenvironment of peptides, proteins and lipid bilayers using intrinsic or extrinsic fluorescent probes.[1] Among the proteinogenic aromatic amino acids only tryptophan shows an evident solvatochromic effect and could be used as such a probe.[1–3] An alternative is application of non-proteinogenic amino acids such as 3-(2-benzoxazol-5-yl)alanine derivatives. Those compounds are fluorescent amino acids whose spectral and photophysical properties are often sensitive to the ambient medium. Moreover, their solvatochromic effect depends on the substituent in position 2.[4–12] In the case of 3-[2-(phenyl)benzoxazol-5-yl]-alanine derivatives, the presence of a substituted amino group in position 4 of the phenyl is mainly responsible for their solvatochromism.[5,9,10,12] How big is this effect depends on the amount and type (aliphatic or aromatic) of substituents on the amino group.[9,10,12] This is mainly due to the fact that the nature of the substituent on the amino group determines the strength of electron-transfer (dependent on the ionization potential) and π-donor ability (coupling of electrons with the residual part of a molecule).[13]

Taking these facts into account we decided to broaden our previous studies on solvatochromism of 3-[2-(4-aminophenyl)-benzoxazol-5-yl]alanine derivatives[9,12] synthesizing such derivatives with *N*-phenylcarbazole substituents and analyzing their spectral and photophysical properties. Such studies allow us to answer the question of how stiffening of substituents on the amino group affects the solvatochromic effect of that

[a]*Faculty of Chemistry, University of Gdańsk, Sobieskiego 18, 80-952 Gdańsk, Poland. E-mail: kasiag@chem.univ.gda.pl; Fax: (+48)-(58)-5235472; Tel: (+48)-(58)-5235413*
[b]*Institute of Experimental Physics, Faculty of Mathematics, Physics and Informatics, University of Gdańsk, Wita Stwosza 57, 80-952 Gdańsk, Poland*

†Electronic supplementary information (ESI) available: Emission spectra of exciplex of compound **2** in dimethoxyethane, results of the single-parameter linear correlations of photophysical parameters of **1** and **2** with E_T^N as well as their multi-parameter linear correlations with three-parameter Catalán and Kamlet–Taft solvent scales, theoretically calculated absorption wavelengths for both compounds studied, their HOMO and LUMO orbitals and orientation of the transition dipole moments as well as the results of fluorescence anisotropy measurements of stretched samples in PVA films. See DOI: 10.1039/c2pp25114k

‡Current address (M. Sz.): Department of Physics and Biophysics, University of Warmia and Mazury in Olsztyn, Oczapowskiego 4, 10-719 Olsztyn, Poland.

compound. Choosing *N*-phenylcarbazole as a substituent results from its important role in the design of compounds for optoelectronics (OLED) and the presence of such a moiety in fluorescent dyes or photosensitive dyes in solar cells[14,15] as well as biologically active compounds.[16]

2 Experimental

2.1 Synthesis

N-Boc-3-[2-(4-(9*H*-carbazolyl)phenyl)benzoxazol-5-yl]alanine methyl ester (**1**) and *N*-Boc-3-[2-(3-(9-phenyl-9*H*-carbazolyl))-benzoxazol-5-yl]alanine methyl ester (**2**) (Fig. 1) were synthesized according to the procedure published previously[4,6–12] based on the oxidative cyclization of the Schiff base obtained from *N*-Boc-3-aminotyrosine methyl ester and the appropriate aldehyde. Moreover, 4-(9*H*-carbazolyl)benzaldehyde and 9-phenyl-9*H*-carbazole-3-carbaldehyde were not commercially available. Because of that the former was obtained by alkylation of carbazole with 4-bromobenzaldehyde[17] whereas the latter by formylation of *N*-phenylcarbazole with 1,1-dichloromethyl methyl ether and $TiCl_4$.[18]

2.1.1 4-(9*H*-Carbazolyl)benzaldehyde. To a magnetically stirred solution of carbazole (0.50 g, 2.99 mmol) in 1,2-dichlorobenzene (12 ml) 4-bromobenzaldehyde (1.80 g, 9.73 mmol), K_2CO_3 (0.99 g, 7.18 mmol), Cu (0.08 g, 1.41 mmol) and 18-crown-6 (0.16 g, 0.61 mmol) were added. The mixture was degassed with argon for about 30 min and then refluxed for about 3 days. After that time, the reaction mixture was cooled down, filtered and evaporated giving a brown oil which was treated with petroleum ether and left overnight with constant magnetic stirring to elute impurities. The ether layer was rejected due to the lack of product and the residue was purified by column chromatography (Merck, Silica gel 60, 0.040–0.063 mm) using a mixture of ethyl acetate–petroleum ether 1 : 15 (v/v) as an eluent. A pale yellow solid was obtained as a product (0.78 g, 2.88 mmol, 96% yield) which was identified by means of ^{1}H NMR (Varian, Mercury 400BB spectrometer (400 MHz) in $CDCl_3$), IR spectra (Bruker IFS-66 instrument) and mass spectra (Bruker Biflex III (MALDI-TOF)).

IR (KBr): ν_{max}/cm^{-1} 3049.0 (ArH), 1702.8 (C═O), 1478.9–1510.8 (C═C); ^{1}H NMR: δ_H (ppm) 7.31–7.49 (6H, m, C$^{7'}$H, C$^{6'}$H, C$^{3'}$H, C$^{2'}$H, C$^{5''}$H, C$^{3''}$H); 7.80 (2H, d, J = 8.0 Hz, C$^{2''}$H, C$^{6''}$H); 8.13–8.16 (4H, m, C$^{8'}$H, C$^{5'}$H, C$^{4'}$H, C$^{1'}$H); 10.12 (1H, s, CHO); MS: m/z = 271.1 (M^+).

2.1.2 9-Phenyl-9*H*-carbazole-3-carbaldehyde. To a magnetically stirred solution of *N*-phenylcarbazole (0.5 g, 2.1 mmol) in 1,2-dichlorobenzene (20 ml) cooled in an ice bath 1,1-dichloromethyl methyl ether (0.24 ml, 2.66 mmol) and $TiCl_4$ (0.36 ml, 3.28 mmol) were added. The reaction was continued for 1 h in the ice bath. Then the reaction mixture was allowed to warm up to the room temperature and poured on ice (200 g) and concentrated HCl (5 ml). The organic layer was diluted with dichloromethane, washed with a 5% solution of HCl and water and dried with anhydrous $MgSO_4$. After evaporation the residue was purified by column chromatography (Merck, Silica gel 60, 0.040–0.063 mm) using a mixture of ethyl acetate–petroleum ether 1 : 15 (v/v) as an eluent, giving the desired compound as a white solid (0.27 g, 1.03 mmol, 49% yield). The product was identified by means of ^{1}H NMR (Varian, Unity plus spectrometer (500 MHz) in $CDCl_3$), IR spectra (Bruker IFS-66 instrument) and mass spectra (Bruker Biflex III (MALDI-TOF)).

IR (KBr): ν_{max}/cm^{-1} 3060.8 (ArH), 1686.1 (C═O), 1436.7–1623.0 (C═C); ^{1}H NMR: δ_H (ppm) 7.39–7.52 (7H, m, C$^{4''}$H, C$^{6''}$H, C$^{3''}$H, C$^{2''}$H, C$^{5''}$H, C$^{1'}$H, C$^{8'}$H), 7.67 (2H, t, J = 7.82 Hz, C$^{6'}$H, C$^{7'}$H), 7.98 (1H, d, J = 8.06 Hz, C$^{2'}$H), 8.24 (1H, d, J = 7.81 Hz, C$^{5'}$H), 8.70 (1H, s, C$^{4'}$H), 10.15 (1H, s, CHO); MS: m/z = 271.1 (M^+).

2.1.3 3-(2-Benzoxazol-5-yl)alanine derivatives – general procedure. A mixture of *N*-Boc-3-nitro-L-tyrosine methyl ester and 10% palladium on active carbon in MeOH was stirred under a hydrogen atmosphere at room temperature for about 90 min (TLC monitoring, Merck silica-gel plates (Kieselgel 60 F_{254}), (CH_2Cl_2–MeOH–AcOH 100 : 10 : 1), R_f = 0.9 (*N*-Boc-3-nitro-L-tyrosine methyl ester), R_f = 0.72 (*N*-Boc-3-amino-L-tyrosine methyl ester)). The catalyst was filtered off and the solvent evaporated to give a brownish oily product which was dissolved in anhydrous EtOH and mixed with the solution of the appropriate aldehyde (1 equiv.) in anhydrous EtOH. The mixture was stirred at RT overnight (TLC monitoring (AcOEt–petroleum ether 1 : 5)). After this time, the solvent was removed by evaporation and the Schiff base obtained (yellow solid) was dissolved in DMSO and lead tetraacetate (1.5 equiv.) was added. The mixture was stirred at RT for about 2 h (TLC monitoring (AcOEt–petroleum ether 1 : 3)) and then dissolved in AcOEt and washed in turn with a saturated aqueous solution of NaCl (1×), a 5% solution of $NaHCO_3$ (2×), a saturated aqueous solution of NaCl (3×), and dried with anhydrous $MgSO_4$. The solvent was evaporated and the product was isolated by means of column chromatography (Merck, Silica gel 60,

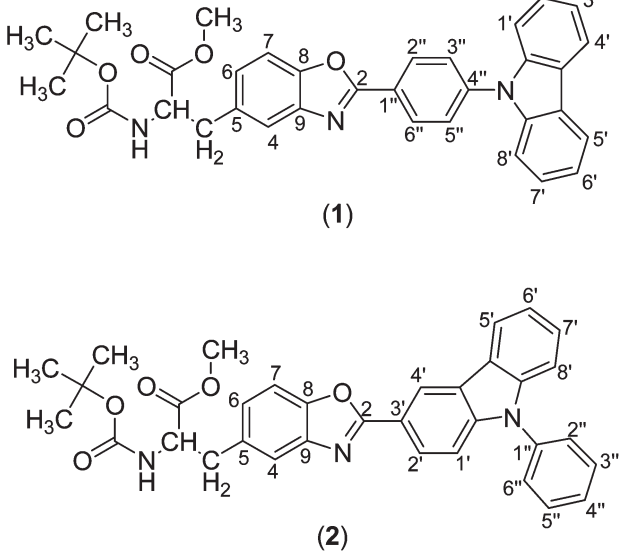

Fig. 1 Structures of compounds studied.

0.040–0.063 mm) using a mixture of AcOEt–petroleum ether 1 : 5 (v/v) (compound **1**) or AcOEt–petroleum ether 1 : 3 (v/v) (compound **2**) as an eluent. The crude products were recrystallized from a mixture of AcOEt–petroleum ether. Compound **1** was obtained as a white solid with 44% yield. In the case of compound **2**, the additional purification by means of RP-HPLC was necessary (gradient 50–100% B over 120 min (A = 0.1% water solution of trifluoroacetic acid, B = 80% of acetonitrile in A), Kromasil column, C-8, 5 μm, 250 mm long, i.d. = 20 mm). It was obtained as a white solid with 10% yield. The purity of the obtained compounds was checked by means of analytical RP-HPLC (compound **1** – Phenomenex® Jupiter column (C18, 5 μm, 250 mm long, i.d. = 4.5 mm), compound **2** – Kromasil column (C-8, 5 μm, 250 mm long, i.d. = 4.5 mm)) with detection at λ = 223 nm. The mobile phase was a gradient running from 0 to 100% of B over 60 min plus 100% of B over 10 min (t_R = 67.4 min (**1**), t_R = 66.8 min (**2**)). The identification of the products was based on the ^{1}H NMR (Varian, Mercury 400 BB (400 MHz) (compound **1**) or Unity 500 plus spectrometer (500 MHz) (compound **2**)) in $CDCl_3$ and mass spectra (Bruker Biflex III (MALDI-TOF)).

Compound **1**: ^{1}H NMR: δ_H (ppm) 1.44 (9H, s, $(CH_3)_3$), 3.19–3.31 (2H, m, $C^{\beta}H_2$), 3.76 (3H, s, OCH_3), 4.67 (1H, d, J = 8.0 Hz, $C^{\alpha}H$), 5.06 (1H, d, J = 8.0 Hz, NH), 7.16–7.19 (1H, m, C^6H), 7.31–7.34 (2H, m, $C^{3'}H$, $C^{6'}H$), 7.42–7.46 (2H, m, $C^{2'}H$, $C^{7'}H$), 7.50–7.54 (4H, m, C^7H, C^4H, $C^{1'}H$, $C^{8'}H$), 7.76–7.78 (2H, m, $C^{3''}H$, $C^{5''}H$), 8.15–8.17 (2H, m, $C^{2''}H$, $C^{6''}H$), 8.47–8.49 (2H, m, $C^{4'}H$, $C^{5'}H$); MS: m/z 562.3 (MH^+).

Compound **2**: ^{1}H NMR: δ_H (ppm) 1.46 (9H, s, $(CH_3)_3$), 3.22–3.31 (2H, m, $C^{\beta}H_2$), 3.77 (3H, s, OCH_3), 4.68 (1H, q, J = 5.9 Hz, J = 13.2 Hz, $C^{\alpha}H$), 5.07 (1H, d, J = 8.3 Hz, NH), 7.14 (1H, dd, J = 2.0 Hz, J = 8.3 Hz, $C^{8'}H$), 7.38 (1H, t, J = 7.8 Hz, C^6H), 7.44 (1H, d, J = 7.8 Hz, C^7H), 7.48–7.56 (6H, m, $C^{3''}H$, $C^{4''}H$, $C^{5''}H$, $C^{6'}H$, $C^{7'}H$, C^4H), 7.61 (2H, dd, J = 1.5 Hz, J = 7.3 Hz, $C^{2''}H$, $C^{6''}H$), 7.67 (1H, t, J = 7.3 Hz, $C^{4'}H$), 8.28 (1H, d, J = 7.3 Hz, $C^{2'}H$), 8.32 (1H, dd, J = 1.5 Hz, J = 8.8 Hz, $C^{5'}H$), 9.08 (1H, d, J = 1.5 Hz, $C^{1'}H$); MS: m/z 561.1 (M^+).

2.2 Spectroscopic measurements

The absorption spectra of **1** and **2** in all solvents studied (22 for **1** and 36 for **2**) were measured with a Perkin-Elmer Lambda 40P spectrophotometer, whereas emission spectra were measured using a Perkin-Elmer LS 50B or a Horiba Jobin Yvon Fluoromax-4 spectrofluorimeter. Solvents of the highest available quality (spectroscopic or HPLC grade) were used.

Fluorescence quantum yields (φ_F) were calculated with quinine sulphate in 0.5 M H_2SO_4 (φ_F = 0.53 ± 0.02) as a reference and were corrected for different refractive indices of solvents.[1] In all fluorimetric measurements, the optical density of solution does not exceed 0.1.

The fluorescence lifetimes were measured with a time-correlated single-photon counting apparatus Edinburgh CD-900. The excitation source was a NanoLed N16 (UV led 339 nm) from IBH. The half-width of the response function of the apparatus was about 1.0 ns using a Ludox solution as a scatter. The emission wavelengths were isolated using a monochromator (about 12 nm spectral band-width). Fluorescence decay data were fitted by the iterative convolution to the sum of exponents according to eqn (1):

$$I(t) = \sum_i \alpha_i \exp(-t/\tau_i) \quad (1)$$

where α_i is the pre-exponential factor obtained from the fluorescence intensity decay analysis and τ_i the decay time of the i-th component, using a software supported by the manufacturer. The adequacy of the exponential decay fitting was judged by visual inspection of the plots of weighted residuals as well as by the statistical parameter X_R^2 and shape of the autocorrelation function of the weighted residuals and serial variance ratio (SVR). For compound **2** in dimethoxyethane additional measurements were made with a picosecond laser excitation using a streak-camera as a detector.[19]

The multiple linear regression, approach of Kamlet and co-workers,[20–23] and Catalán and co-workers,[24–27] has been used to correlate UV–Vis absorption and emission energies with an index of the solvent dipolarity/polarizability which is a measure of the solvent's ability to stabilize a charge or dipole through nonspecific dielectric interactions (π* or SPP), and indices of the solvent's hydrogen-bond donor strength (α or SA) and hydrogen-bond acceptor strength (β or SB) according to eqn (2) and (3):

$$\nu_{A,F} = \nu_0 + a_{\pi*} \times \pi* + b_\alpha \times \alpha + c_\beta \times \beta \text{ Kamlet–Taft equation} \quad (2)$$

or

$$\nu_{A,F} = \nu_0 + a_{SPP} \times SPP + b_{SA} \times SA + c_{SB} \times SB \text{ Catalán equation} \quad (3)$$

Moreover, a similar correlation was performed using Catalán's new generalized solvent polarity empirical scale splitting the SPP parameters for two components: SP – solvent polarizability and SdP – solvent dipolarity. Mathematically, this scheme is formulated as follows:

$$y = y_0 + a_{SP} \times SP + b_{SdP} \times SdP + c_{SA} \times SA + d_{SB} \times SB \quad (4)$$

where y denotes a solvent-dependent physicochemical property in a given solvent and y_0 the statistical quantity corresponding to the value of the property in the gas phase; SP, SdP, SA, SB represent independent solvent parameters accounting for various types of solute–solvent interactions; a_{SP}, b_{SdP}, c_{SA} and d_{SB} are adjustable coefficients that reflect the sensitivity of physical property y in a given solvent to the various solvent parameters.[28]

Based on spectroscopic data the excited state dipole moment of molecules studied was determined using eqn (5) and (6) from the Kawski's theory:[29–32]

$$\tilde{\upsilon}_a - \tilde{\upsilon}_f = m_1 f(\varepsilon_r, n) + \text{const} \quad (5)$$

$$\tilde{\upsilon}_a + \tilde{\upsilon}_f = -m_2[f(\varepsilon_r, n) + 2g(n)] + \text{const} \quad (6)$$

where $\tilde{\upsilon}_a$ and $\tilde{\upsilon}_f$ are the absorption and emission band maximum (in wavenumbers), respectively, measured in solvents of different relative permittivities ε_r and different refractive indices n. The solvent polarity functions $f(\varepsilon_r, n)$ and $g(n)$ are given by eqn (7) and (8):

$$f(\varepsilon_r, n) = \frac{2n^2+1}{n^2+2}\left(\frac{\varepsilon-1}{\varepsilon+2} - \frac{n^2-1}{2n^2+1}\right) \quad (7)$$

$$g(n) = \frac{3(n^4-1)}{2(n^2+2)^2} \quad (8)$$

Using a slope obtained from eqn (5) and (6) and knowing the ground state dipole moment, the excited state dipole moment can be calculated using eqn (9) and (10) as well as an angle ψ between them (eqn (11) and (12)):

$$m_1 = \frac{(\vec{\mu}_e - \vec{\mu}_g)^2}{2\pi\varepsilon_0 hca^3} = \frac{(\mu_e^2 + \mu_g^2 - 2\mu_e\mu_g\cos\Psi)}{2\pi\varepsilon_0 hca^3} \quad (9)$$

$$m_2 = \frac{(\mu_e^2 - \mu_g^2)}{2\pi\varepsilon_0 hca^3} \quad (10)$$

$$\mu_e = \sqrt{(\mu_g^2 + \frac{1}{2}m_2 hca^3)} \quad (11)$$

$$\cos\Psi = \frac{1}{2\mu_e\mu_g}\left[(\mu_g^2 + \mu_e^2) - \frac{m_1}{m_2}(\mu_e^2 - \mu_g^2)\right] \quad (12)$$

where μ_e and μ_g are the dipole moments in the excited and ground states, respectively, a is Onsager's interaction radius of the solute, h is the Planck's constant (6.626×10^{-34} Js), c is the velocity of light in a vacuum (3×10^8 ms^{-1}), ε_0 is the permittivity of vacuum (8.85×10^{-12} V C^{-1} m^{-1}), thus $2\pi\varepsilon_0 hc$ = $1.105110440 \times 10^{-35}$ C^2. If the ground and excited state dipole moments are parallel, based on eqn (9) and (10), eqn (13)–(15) can be derived:

$$\mu_g = \frac{m_2 - m_1}{2}\sqrt{\frac{hca^3}{2m_1}} \quad (13)$$

$$\mu_e = \frac{m_2 + m_1}{2}\sqrt{\frac{hca^3}{2m_1}} \quad (14)$$

or

$$\mu_e = \mu_g\frac{m_1 + m_2}{m_2 - m_1} \qquad \text{for} \quad m_2 > m_1 \quad (15)$$

The angles between absorption and fluorescence transition moments of the compounds studied were calculated using the Kawski–Gryczyński method[33–37] based on fluorescence polarization measurements (λ_{ex} = 330 nm) in stretched poly(vinyl alcohol) (PVA) films. Each compound was dissolved in a 5% water–methanol mixture of PVA (M ~ 205 000) at 340 K to obtain a homogeneous solution. The samples were left for several days for evaporation to obtain thin PVA films which were then uniaxially stretched. As mechanical stretching gives the control over the degree of orientation of transition dipole moments through the correlation with respective distribution functions of the fluorophore in a partly ordered PVA matrix,[33–36,38–40] ten samples of different stretching factors were prepared using a standard procedure and equipment developed earlier.[37,38]

2.3 Quantum chemical calculations

The structures of all calculated compounds were prepared and initially optimized using the Avogadro program applying the UFF force field method.[41] All calculations were performed at the DFT level with the hybrid functional pbe0 using TURBOMOLE package (version 5.9). The geometry optimization was carried out without symmetry constraints, using a def2-TZVP basis set. This procedure was considered satisfactory if the energy difference between optimized cycles was $<1 \times 10^{-6}$ Hartree and a gradient of $<1 \times 10^{-3}$ au was achieved. The low-lying excited states were treated within the adiabatic approximation of time-dependent density functional theory (DFT-RPA) using a pbe0 functional. The geometry optimization of excited states was performed using a grid parameter equal to 4. The convergence of all systems studied was checked by harmonic vibrational analysis. No imaginary frequencies were observed. In addition, TD DFT calculation was carried out at the geometry of the ground state for the first 20 transitions in order to simulate the absorption spectrum in the Franck–Condon region. In order to take into account the influence of the solvent effects on the geometry and spectral shifts of UV–vis spectra, all calculations were carried out using the COSMO model implemented in the TURBOMOLE program. The calculated absorption energies and intensities were transformed with the GaussSum program into simulated spectra using Gaussian functions assuming a constant bandwidth at the half-height of 4000 cm^{-1}. This value constitutes an average width for an absorption band observed in the UV–Vis range.

3 Results and discussion

Both benzoxazol-5-ylalanine derivatives studied (Fig. 1) possess as a substituent in position 2 an *N*-phenylcarbazole subunit, but differently connected to the benzoxazole moiety – for *N*-Boc-3-[2-(4-(9*H*-carbazolyl)phenyl)benzoxazol-5-yl]alanine methyl ester (**1**) by phenyl whereas for *N*-Boc-3-[2-(3-(9-phenyl-9*H*-carbazolyl))benzoxazol-5-yl]alanine methyl ester (**2**) by carbazole. This is probably a reason for observed significant differences between the compounds studied in their spectral and photophysical properties.

The absorption spectra of both compounds studied in selected solvents are shown in Fig. 2, whereas in Fig. 3 their emission spectra are presented. For both compounds the absorption band with a maximum at about 340 nm overlaps with the absorption band assigned to the $S_2 \leftarrow S_0$ and/or $S_3 \leftarrow S_0$ transition of phenylcarbazole.[42,43] This band is shifted to about 305 nm for compound **2** and to about 290 nm for **1**, indicating a bigger overlap with the main absorption band for **2**. A more pronounced vibrational structure is observed for **1** in saturated hydrocarbon solvents. In more polar solvents, the

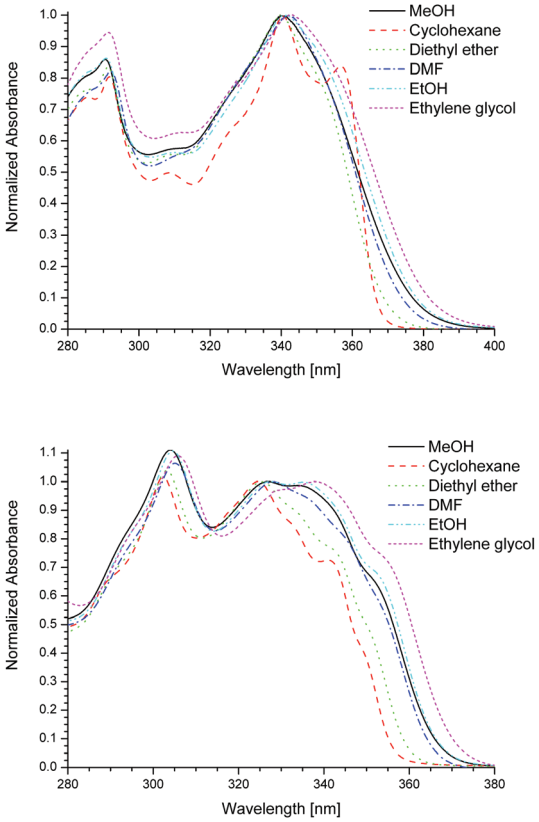

Fig. 2 Normalized absorption spectra of **1** (at the top) and **2** (at the bottom) in selected solvents.

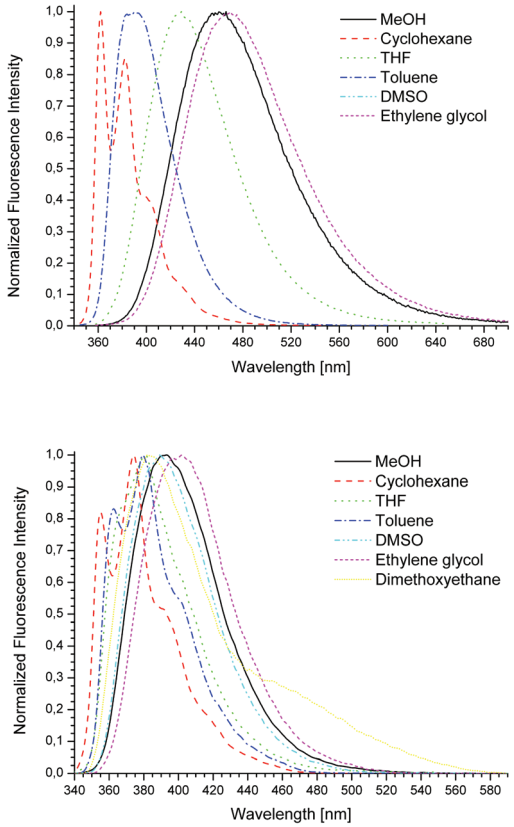

Fig. 3 Normalized emission spectra of **1** (at the top) and **2** (at the bottom) in selected solvents.

absorption spectra of both compounds shift. Moreover, the band's shape changes and its vibrational structure becomes diffuse. All these changes are more distinct for compound **2**. A bigger shift of the absorption band indicates that the change of the dipole moment between the ground and Franck–Condon states is larger for **2** than for **1**.

The influence of the solvent is greater in the case of fluorescence spectra of both compounds (Fig. 3). However, the emission maxima of compound **2** are shifted to the red to a lesser degree than those of compound **1** indicating that **1** has a larger dipole moment in the excited state than **2**. Also, the vibrational structure of fluorescence spectra is more pronounced for **1** than for **2** as the structure of **1** is probably more stiffened. It is a result of charge transfer between the substituent (*N*-phenylcarbazole) and the benzoxazole moiety causing increase of the electron density on $C_{benzoxazole}$–C_{Ph} and C_{Ph}–$N_{carbazole}$ bonds which become multiple bonds instead of single. This indicates that the electron-donating property of the phenylcarbazole substituent depends on the position of substitution.

The photophysical properties of compounds **1** and **2** are compiled in Tables 1 and 2, respectively. As shown in Table 1, the fluorescence quantum yield of **1** is high (close to unity in cyclohexane) to moderate (0.36 in methanol) and depends on the solvent polarity. A similar dependence is observed for the fluorescence lifetimes of **1**. The longest fluorescence lifetimes, close to the fluorescence lifetime of *N*-phenylcarbazole in air-saturated solvents,[42,43] are observed in polar and protic solvents (6.17 ns in ethylene glycol, 5.45 ns in DMSO), whereas in hydrocarbon solvents they are shorter (1.30 ns in isooctane). For **2** the fluorescence quantum yields are also high and close to unity in polar and protic solvents and only a little lower in saturated hydrocarbon solvents (Table 2). The fluorescence lifetimes of **2** are much shorter (from 1.3 ns in chloroform to 2.7 ns in *n*-pentane) than that for 3-substituted carbazole.[44] Both fluorescence quantum yields and fluorescence lifetimes of **2** only slightly depend on solvent polarity. In most solvents mono-exponential fluorescence intensity decays are observed for both derivatives. For **1**, multi-exponential fluorescence intensity decays are observed in THF, 2-methyl-THF, diethyl ether, *n*-hexanol, *n*-heptanol and propylene glycol, whereas for **2** only in dimethoxyethane. In the case of **1**, the presence of additional fluorescence lifetime (shorter one) is caused by specific interaction between the solute and these solvents. For aprotic solvents, this component may be connected with formation of a complex with solvent possessing lone electron pairs at the oxygen atom (charge-transfer type complexes), whereas for protic ones it is probably a result of specific solvation of **1** by alcohols with suitably long hydrocarbon chains. In the case of **2**, its fluorescence spectrum in dimethoxyethane possesses a long-wavelength shoulder, probably connected with formation of an excited state complex with the solvent

Table 1 Spectroscopic and photophysical properties of **1** in all solvents studied

Solvent	$\tilde{\nu}_{abs}$ [cm^{-1}]	$\tilde{\nu}_{fluo}$ [cm^{-1}]	φ_F	τ [ns]	α	χ_R^2	$\Delta\tilde{\nu}$ [cm^{-1}]	$k_f/10^8$ [s^{-1}]	$k_{nr}/10^7$ [s^{-1}]
Methanol	29 438	21 460	0.36	5.34	1.00	1.03	7979	0.68	11.97
Ethanol	29 370	22 472	0.63	5.30	1.00	1.17	6897	1.18	7.04
1-Butanol	29 257	23 256	0.69	4.52	1.00	1.16	6001	1.53	6.79
tert-Buthyl alcohol	29 257	23 753	0.81	4.03	1.00	1.08	5504	2.00	4.76
iso-Propyl alcohol	29 370	23 202	0.59	4.49	1.00	1.17	6167	1.32	9.04
Amyl alcohol	29 343	24 450	0.77	3.36	1.00	1.08	4893	2.29	6.90
n-Hexanol	29 189	23 585	0.73	4.11	1.00	2.44	5604	—	—
				4.21	0.60	1.10			
				0.39	0.40				
n-Heptanol	29 197	23 697	0.65	4.00	1.00	3.74	5500	—	—
				4.15	0.52	1.10			
				0.42	0.48				
Ethylene glycol	29 137	21 276	0.52	6.17	1.00	1.06	7861	1.78	6.57
Propylene	29 214	21 978	0.55	5.74	1.00	3.25	7236	—	—
Glycol				5.9	0.68	1.13			
				0.71	0.32				
Acetone	29 351	23 095	0.44	4.28	1.00	1.07	6436	1.03	13.06
Acetonitrile	29 412	22 371	0.46	5.02	1.00	1.10	7040	0.91	11.95
Cyclohexane	29 412	27 624	0.94	1.37	1.00	1.15	1788	6.88	4.16
Isooctane	29 420	27 700	0.55	1.30	1.00	1.11	1720	4.19	35.00
1,4-Dioxane	29 291	25 000	0.62	2.49	1.00	1.14	4291	2.49	15.26
THF	29 257	23 310	0.53	3.32	1.00	3.98	5947	—	—
				3.55	0.60	1.09			
				0.67	0.40				
2-Methyl-	29 290	24 752	0.52	2.78	1.00	1.59	4539	—	—
THF				1.14	0.19	1.00			
				2.91	0.81				
Diethyl	29 446	24 856	0.56	2.80	1.00	2.59	4570	—	—
Ether				0.76	0.30	1.07			
				2.95	0.70				
Toluene	29 188	25 575	0.69	1.84	1.00	1.14	3613	3.77	16.68
Ethyl acetate	29 410	24 450	0.54	3.08	1.00	1.12	4962	1.76	14.90
DMF	29 230	22 830	0.58	4.97	1.00	1.13	6400	1.17	8.53
DMSO	29 104	22 422	0.47	5.45	1.00	1.10	6682	0.86	9.74

molecules (Fig. 1S, ESI†) which was confirmed by time-resolved measurements. The fluorescence intensity decays of **2** in dimethoxyethane measured at 370 nm and 500 nm are bi-exponential in both cases, however, a negative pre-exponential factor (the growth of fluorescence intensity) is observed for measurement at λ = 500 nm (Table 2). The exciplex formation with a solvent molecule is also confirmed by time-resolved spectra (Fig. 2S, ESI†).

The solvatochromic properties were applied also to the calculations of excited state dipole moments of the compounds studied using eqn (5) to (15), presented in the experimental section. In these studies we accept the condition $2\alpha/a^3 = 1$, frequently adopted in the literature, and solvent polarity functions represented by eqn (7) and (8) were used.

To calculate the excited state dipole moment the ground state dipole moment is necessary. For both compounds, they were obtained from the theoretical calculation performed by applying a DFT method with a def2-TZVP basis set (TURBOMOLE v. 5.9) (2.6 D for **2** and 1.6 D for **1**). The smaller value of the ground state dipole moment for **1** is probably caused by nonplanarity of the *N*-phenylcarbazole moiety and the benzoxazole ring resulting in weaker interaction between them.[13,42] In the case of **2**, the carbazole subunit can adopt planar orientation with the rest of the molecule, as it is not separated by the phenyl, yielding a higher ground state dipole moment value.

The calculations of excited state dipole moment values were performed taking into account only solvents in which mono-exponential fluorescence decays were observed without a division on protic or aprotic ones. The correlations of spectral properties with solvent polarity-polarizability functions according to eqn (5) and (6) are satisfactory for **1** (r = 0.9728 for eqn (5) and r = 0.9682 for eqn (6), Table 3). The calculated excited state dipole moment is equal to 8.7 D whereas an angle between the ground and excited state dipole moments is 56.5°. For **2**, these correlations are much poorer (r = 0.5921 for eqn (5) and r = 0.7514 for eqn (6), Table 3) giving an excited state dipole moment value equal to 5.4 D with parallel orientation of the ground and excited state dipole moments. In such a case the ground state dipole moment can be calculated from eqn (13) and the value of 2.7 D, comparable to the theoretically calculated value (2.6 D), was obtained. Moreover, based on eqn (15), the excited state dipole moment can be calculated only from the spectroscopic properties without taking into account the Onsager's radius and for **2** it is equal to 5.4 D, exactly as obtained from eqn (11).

The spectroscopic and photophysical properties of **2** and to a less degree those of **1** depend on whether the solvent is protic or aprotic. Thus, the excited state dipole moments were also calculated taking into account only aprotic solvents to exclude the influence of hydrogen bond formation between

Table 2 Spectroscopic and photophysical properties of **2** in all solvents studied

Solvent	$\tilde{\nu}_{abs}$ [cm^{-1}]	$\tilde{\nu}_{fluo}$ [cm^{-1}]	φ_F	τ [ns]	α	χ_R^2	$\Delta\tilde{\nu}$ [cm^{-1}]	$k_f/10^8$ [s^{-1}]	$k_{nr}/10^7$ [s^{-1}]
Methanol	29 922	25 455	0.99	1.72	1.00	0.98	4537	5.76	0.58
Ethanol	29 878	25 641	1.00	1.66	1.00	1.24	4237	6.02	0
1-Butanol	30 544	25 940	1.10	1.54	1.00	1.07	4604	6.49	0
Iso-Butyl alcohol	29 780	25 974	1.00	1.55	1.00	0.85	3806	6.45	0
Iso-Propyl alcohol	30 581	26 008	1.00	1.57	1.00	1.02	4573	6.37	0
Amyl alcohol	30 553	26 247	1.00	1.54	1.00	1.15	4306	6.49	0
n-Hexanol	30 469	25 907	0.94	1.56	1.00	1.17	4589	6.03	3.85
Cyclohexanol	30 432	26 042	0.95	1.58	1.00	0.96	4390	6.01	3.16
n-Heptanol	30 460	26 110	1.00	1.55	1.00	1.00	4350	6.45	0
Ethylene glycol	29 507	25 189	1.00	1.84	1.00	1.11	4318	5.43	0
Propylene glycol	29 586	25 221	1.00	1.74	1.00	0.94	4365	5.75	0
Formamide	30 516	24 752	0.82	1.86	1.00	1.08	5764	4.41	9.68
Acetone	30 684	26 385	0.63	1.75	1.00	1.06	4299	3.60	21.14
Acetonitrile	30 684	26 178	0.99	1.77	1.00	1.13	4506	5.59	0.56
Chloroform	30 331	26 008	0.93	1.32	1.00	1.05	4323	7.05	5.30
Methylene chloride	30 414	26 178	0.94	1.50	1.00	1.15	4236	6.27	4.00
n-Pentane	30 817	26 846	0.59	2.66	1.00	1.00	3971	2.21	15.41
3-Methyl-pentane	30 826	26 846	0.59	2.25	1.00	1.03	3980	2.62	18.22
Cyclohexane	30 675	26 740	0.76	2.29	1.00	0.91	3935	3.32	10.48
n-Hexane	30 741	26 810	0.58	2.23	1.00	0.96	3931	2.61	18.83
Isooctane	30 760	26 810	0.86	2.22	1.00	1.09	3950	3.87	6.31
n-Nonane	30 675	26 702	0.72	2.30	1.00	1.06	3973	3.13	12.17
n-Decane	30 656	26 738	0.75	2.33	1.00	1.00	3918	3.22	10.73
Dimethoxyethane	30 600	26 178	0.70	1.20	1.00	1.52[a]	4422	—	—
				1.14	0.97	1.09[a]			
				2.20	0.03				
				4.27	1.00	18.49[b]			
				1.08	−2.73				
				3.93	3.73	1.08[b]			
1,4-Dioxane	30 553	26 350	1.00	1.96	1.00	1.01	4203	5.10	0
THF	30 554	26 281	0.84	1.73	1.00	0.91	4273	4.86	9.25
2-Methyl-THF	30 590	26 385	0.93	1.83	1.00	1.20	4205	5.08	3.82
Diethyl Ether	30 741	26 560	0.68	2.13	1.00	0.99	4181	3.19	15.02
Di-isopropyl ether	30 544	26 008	0.55	1.66	1.00	0.83	4536	3.31	27.11
Propylene carbonate	30 675	26 469	1.00	1.83	1.00	1.36	4206	5.46	0
Benzene	30 414	26 281	0.97	1.67	1.00	1.08	4133	5.81	1.79
Toluene	30 404	26 350	0.78	1.66	1.00	1.04	4054	4.70	13.25
o-Xylene	30 386	26 350	0.92	1.76	1.00	0.97	4036	5.23	4.54
Ethyl acetate	30 713	26 420	0.96	1.87	1.00	0.94	4293	5.13	2.14
DMF	30 497	26 008	1.00	1.73	1.00	1.07	4489	5.78	0
DMSO	30 066	25 707	0.88	1.69	1.00	1.10	4359	5.21	7.10

Measured at[a] λ_{em} = 370 nm, [b] λ_{em} = 500 nm.

Table 3 Ground state dipole moments (μ_g), the slopes of linear fits (m_1) and (m_2) obtained from the fitting of Stokes shift (eqn (5)) and sum of absorption and emission maxima (eqn (6)) *versus* solvent polarity functions, regression coefficient (r) (representing the quality of fit), excited state dipole moments (μ_e), the angle between ground and excited state dipole moments (ψ) and changes of dipole moments calculated from the dependence of the Stokes shift on the E_T^N parameter (eqn (16))

Compound	μ_g [D]	a [Å]	m_1	r_{m1}	m_2	r_{m2}	μ_e [D]	Ψ	$\Delta\mu$ [D]	Comment
1	1.6	6.0	5098 ± 243	0.9728	−(6784 ± 350)	0.9682	8.7	56.5	6.1	All solvents
			5188 ± 215	0.9857	−(6787 ± 329)	0.9806	8.7	53.3	8.3	Aprotic
									6.9	Protic
2	2.6	6.5	574 ± 136	0.5921	−(1626 ± 245)	0.7514	5.4	0.0	2.7	All solvents
			670 ± 83	0.8644	−(1175 ± 209)	0.7606	4.8	34.3	3.9	Aprotic
									4.6	Protic

the solute and the solvent. It was found that exclusion of protic solvents does not change much parameters obtained for **1** in contrast to compound **2** (Table 3). The quality of fit for **2** is much better, especially for eqn (5) (r = 0.8644). The calculated excited state dipole moment for aprotic solvents is now a bit lower (μ_e = 4.8 D), while the angle between dipoles substantially increases to the value of 34.3° (Table 3).

To calculate the dipole moment change between the excited and ground states, the correlation of the Stokes shift with the microscopic solvent polarity parameter E_T^N can be applied.[45,46]

According to the equation proposed by Ravi *et al.*,[45] the problem associated with the Onsager's radius estimation can be minimized since a ratio of two Onsager's radii is involved:

$$\Delta\tilde{\upsilon} = \tilde{\upsilon}_a - \tilde{\upsilon}_f = 11307.6\left[\left(\frac{\Delta\mu}{\Delta\mu_B}\right)^2\left(\frac{a_B}{a}\right)^3\right]E_T^N + \text{const} \qquad (16)$$

where $\Delta\mu_B$ and a_B are the dipole moment change ($\Delta\mu = \mu_e - \mu_g$) and Onsager's radius, respectively for a pyridinium *N*-phenolate betaine dye used to determine the E_T^N values ($\Delta\mu_B$ = 9 D and a_B = 6.2 Å), whereas $\Delta\mu$ and a are the corresponding quantities for the molecule under study. Calculated according to eqn (16) dipole moment changes are presented in Table 3. The excited state dipole moments calculated taking into account all solvents are comparable to the values obtained from the Kawski's theory, however, excited state dipole moments calculated only for aprotic solvents appear to be overestimated.

3.1 Single parameter correlation

Absorption maximum (in wavenumber), fluorescence maximum (in wavenumber), Stokes shift, fluorescence quantum yield as well as fluorescence lifetime of the compounds studied were also correlated with the E_T^N solvent polarity parameter using an equation: $y = y_0 + b \times E_T^N$ (Tables 1S and 2S (ESI†) for compounds **1** and **2**, respectively). Generally, the values of correlation coefficients are rather small indicating the weak or lack of correlation with the E_T^N parameter regardless of whether it is a whole set of solvents studied, or after the division on protic and aprotic ones. Moreover, for protic solvents the correlation coefficient is always lower than that for the aprotic ones, except for the fluorescence quantum yield of **1** and the fluorescence lifetime of **2**. The increase of the correlation coefficient for protic or aprotic solvents compared to that for all set of solvents indicates that the partition of solvents on these two groups in most cases is justified.

3.2 Multi-linear correlations

Multi-parameter correlation is preferable and has been applied successfully to various physicochemical parameters. The most frequently used solvent scales are those of Kamlet and Taft,[20–23] and Catalán.[24–28] As Filarowski *et al.*[47] and Guzow *et al.*[12] demonstrated, the new four-parameter Catalán solvent scale has an advantage over other solvent scales. Therefore, in this manuscript the spectral and photophysical parameters of the compounds studied in all solvents used will be discussed based on the four-parameter Catalán solvent scale.[28] However, the correlations obtained using Kamlet–Taft and an old three-parameter Catalán solvent scale are also presented (Tables 3S–6S, ESI†) and will be compared with each other.

Table 4 collects the estimated coefficients and correlation coefficients (r) for the multi-linear regression analysis of absorption ($\tilde{\nu}_{abs}$) and fluorescence ($\tilde{\nu}_{fluo}$) maxima, fluorescence quantum yield (φ_F) and Stokes shift ($\Delta\tilde{\nu}$) of **1** using the four-parameter Catalán solvent polarity scale (data obtained for three-parameter Catalán or Kamlet–Taft solvent polarity scales are collected in Tables 3S and 4S, ESI†). A fair fit was obtained for the dependence of maxima of absorption ($\tilde{\nu}_{abs}$) (r = 0.9387) in which all four coefficients are important. However, the large value of the a_{SP} coefficient compared to others (b_{SdP}, c_{SA} and d_{SB}) (Table 4) indicates that the change of ($\tilde{\nu}_{abs}$) may reflect primarily a change in polarizability of the environment of the chromophore, whereas the solvent dipolarity (b_{SdP}), because of its low value and large error, may be disregarded (quality of the fit decreases a little (r = 0.9378) compared to the original fit (r = 0.9387)). Solvent acidity and basicity affect the position of the absorption maxima but to a smaller degree than its polarizability. For compound **2**, the analysis of ($\tilde{\nu}_{abs}$) according to eqn (4) (Table 5) indicates that ($\tilde{\nu}_{abs}$) is affected by all four parameters, however, the greatest impact is exhibited by polarizability of the environment of the chromophore, as for compound **1**. The influence of solvent acidity and basicity on ($\tilde{\nu}_{abs}$) is bigger for **2** than for **1**. Similar dependences reflect the correlation of ($\tilde{\nu}_{abs}$) with the three-parameter solvent polarity

Table 4 Estimated from eqn (4) coefficients (y_o, a_{SP}, b_{SdP}, c_{SA}, d_{SB}), their standard errors and correlation coefficients (r) for the multiple linear regression analysis of $\tilde{\nu}_{abs}$, $\tilde{\nu}_{fluo}$, $\Delta\tilde{\nu}$, φ_F, k_f, k_{nr} of **1** as a function of the Catalán four-parameter solvent scale

y	y_0	a_{SP}	b_{SdP}	c_{SA}	d_{SB}	r
$\tilde{\nu}_{abs}$	30 437 ± 107	−(1552 ± 154)	17 ± 36	−(67 ± 46)	−(111 ± 44)	0.9387
	30 433 ± 104	−(1539 ± 148)		−(62 ± 43)	−(103 ± 40)	0.9378
$\tilde{\nu}_{fluo}$	28 032 ± 1389	−(1208 ± 2004)	−(4470 ± 468)	−(2292 ± 595)	−(258 ± 571)	0.9623
	27 144 ± 264		−(4595 ± 409)	−(2347 ± 593)		0.9610
$\Delta\tilde{\nu}$	2405 ± 1373	−(344 ± 1081)	4487 ± 462	2225 ± 589	147 ± 565	0.9617
	2218 ± 257		4518 ± 399	2283 ± 526		0.9614
φ_F	0.37 ± 0.25	0.50 ± 0.36	−(0.37 ± 0.08)	0.06 ± 0.11	0.19 ± 0.10	0.7501
	0.38 ± 0.24	0.48 ± 0.35	−(0.36 ± 0.08)		0.20 ± 0.10	0.7437
τ^*10^9	0.35 ± 1.11	1.27 ± 1.60	3.60 ± 0.37	2.39 ± 0.47	−(0.15 ± 0.45)	0.9644
	1.15 ± 0.21		3.57 ± 0.33	2.30 ± 0.43		0.9627
$k_f \times 10^{-8}$	3.84 ± 1.75	1.87 ± 2.52	−(3.69 ± 0.58)	−(0.09 ± 0.76)	−(1.46 ± 0.71)	0.9186
	5.23 ± 0.56		−(3.20 ± 1.03)		−(2.43 ± 1.73)	0.9073
$k_f/(n^2\tilde{\upsilon}_{fluo}^3) \times 10^5$	1.12 ± 0.35	0.19 ± 0.51	−(0.77 ± 0.11)	−(0.01 ± 0.15)	−(0.17 ± 0.14)	0.9160
	1.20 ± 0.07		−(0.84 ± 0.09)			0.9045
$k_{nr} \times 10^{-8}$	4.25 ± 3.15	−(3.41 ± 4.64)	−(0.73 ± 1.26)	1.03 ± 15.18	0.03 ± 1.88	0.4985

Table 5 Estimated from eqn (4) coefficients (y_o, a_{SP}, b_{SdP}, c_{SA}, d_{SB}), their standard errors and correlation coefficients (r) for the multiple linear regression analysis of $\tilde{\nu}_{abs}$, $\tilde{\nu}_{fluo}$, $\Delta\tilde{\nu}$, φ_F, τ, k_f, k_{nr} of **2** as a function of the Catalán four-parameter solvent scale

y	y_0	a_{SP}	b_{SdP}	c_{SA}	d_{SB}	r
$\tilde{\nu}_{abs}$	32 345 ± 504	−(2484 ± 736)	−(327 ± 179)	−(843 ± 250)	−(489 ± 199)	0.7384
$\tilde{\nu}_{fluo}$	28 032 ± 211	−(2241 ± 309)	−(583 ± 75)	−(1376 ± 105)	63 ± 83	0.9785
	28 093 ± 194	−(2100 ± 291)	−(552 ± 63)	−(1356 ± 101)		0.9781
$\Delta\tilde{\nu}$	4313 ± 528	−(460 ± 772)	910 ± 188	523 ± 263	−(553 ± 208)	0.7744
	4003 ± 89		860 ± 167	533 ± 260	−(513 ± 195)	0.7713
φ_F	0.27 ± 0.24	0.69 ± 0.35	0.10 ± 0.09	0.17 ± 0.12	0.11 ± 0.10	0.6696
	0.27 ± 0.23	0.79 ± 0.33		0.32 ± 0.10		0.5899
$\tau \times 10^9$	3.40 ± 0.41	−(1.79 ± 0.60)	−(0.28 ± 0.14)	0.02 ± 0.22	−(0.42 ± 0.16)	0.7954
	3.40 ± 0.40	−(1.80 ± 0.58)	−(0.28 ± 0.14)		−(0.41 ± 0.15)	0.7954
$k_f \times 10^{-8}$	−2.22 ± 1.78	8.45 ± 2.61	1.11 ± 0.62	1.47 ± 0.91	1.30 ± 0.71	0.8067
$k_f/(n^2\tilde{\nu}^3_{fluo}) \times 10^5$	0.11 ± 0.50	1.18 ± 0.73	0.49 ± 0.17	0.70 ± 0.26	0.30 ± 0.20	0.7129
$k_{nr} \times 10^{-8}$	3.57 ± 1.23	−3.51 ± 1.80	−0.44 ± 0.43	−1.42 ± 0.65	−0.21 ± 0.49	0.6696
	3.79 ± 1.14	−4.19 ± 1.64		−1.97 ± 0.53		0.6349

scales (Tables 3S–6S, ESI†), however, the qualities of fits are much worse.

The fit of ($\tilde{\nu}_{fluo}$) as a function of SP, SdP, SA, SB is satisfactory, as judged by the value of r as the quality-of-fit criterion, for both compounds studied (r = 0.9632 and r = 0.9785 for **1** and **2**, respectively). However, contrary to the fit of ($\tilde{\nu}_{abs}$), the estimated coefficients determining the influence of solvent polarizability and basicity for **1** are calculated with a considerable standard error a_{SP} = −(1208 ± 2004) and d_{SB} = −(258 ± 571), higher than the coefficient value, and can be omitted. The fit according to eqn (4) with (SdP and SA) as independent variables has a correlation coefficient (r = 0.9610) that is nearly the same as for the original fit (r = 0.9623). Also, it is worth mentioning that the b_{SdP} and c_{SA} coefficient values are negative meaning that their changes cause red-shift of the fluorescence maximum. Also, they are higher, taking into account their absolute values, than those calculated for the absorption. This indicates that the electronic structure of the Franck–Condon and relaxed excited state of **1** differ significantly, and the relaxed excited state is more polar, which is consistent with a higher excited state dipole moment than the ground state. For compound **2**, the greatest impact on ($\tilde{\nu}_{fluo}$) is exhibited by solvent polarizability and dipolarity (almost equally), and acidity. Because of a small value and a large standard error of solvent basicity (d_{SB}), it can be omitted in the correlation without changing the quality of the fit (r = 0.9781 compared to r = 0.9785 for the original fit). The values of coefficients influencing ($\tilde{\nu}_{fluo}$) and ($\tilde{\nu}_{abs}$) are comparable indicating that the electronic structures of the Franck–Condon and relaxed excited states of **2** are similar and the relaxed excited state is only slightly more polar, which is consistent with a small change in dipole moment values. Application of the three-parameter solvent scale gives similar dependences but worse qualities of the correlation for **2** contrary to **1** for which the correlation is very good and all three parameters influence the position of the fluorescence maximum significantly (Tables 3S–6S, ESI†).

Correlation of the Stokes shift of **1** with the four-parameter solvent scale gives the same results as for ($\tilde{\nu}_{fluo}$) (Table 4). In the case of **2**, such correlation is weak, probably because of the difficulties in the correct estimation of the ($\tilde{\nu}_{abs}$), and reveals that the SP parameter does not influence the Stokes shift (Table 5). For both compounds, the correlations with three-parameter solvent scales give worse fits and indicate a negligible influence of basicity of the solvent (Tables 3S–6S, ESI†).

The correlation of the fluorescence quantum yield of **1** with SP, SdP, SA, SB as independent variables gives a rather weak fit (r = 0.7501, Table 4). Moreover, it indicates that solvent acidity does not influence the fluorescence quantum yield whereas the solvent polarizability increases while solvent dipolarity decreases the fluorescence quantum yield to a similar degree. Also, for **2** a weak correlation of the fluorescence quantum yield with solvent polarity parameters (eqn (4)) was obtained (r = 0.6696), however, in this case solvent dipolarity and basicity have no impact on it. The same conclusion, for both compounds, can be drawn from the correlations by applying three-parameter solvent scales (Tables 3S–6S, ESI†).

For both compounds studied, the decay of fluorescence intensity can be described as a mono-exponential function, except for the previously discussed solvents, thus, further analysis including the dependence of fluorescence lifetime, fluorescence rate constant and radiationless rate constant on solvent polarity parameters can be performed. The correlation according to eqn (3) and (4) of the fluorescence lifetimes of **1** is satisfactory as in the case of ($\tilde{\nu}_{fluo}$) and the same solvent parameters have a decisive impact (Tables 4, 3S and 4S, ESI†). For **2**, the correlation according to eqn (4) is better (Table 5) than in the case of three-parameter solvent scales (Tables 5S and 6S, ESI†). However, the solvent acidity can be omitted for Catalán four-parameter and Kamlet–Taft solvent scales (Table 5 and Table 6S, ESI†).

For the mono-exponential fluorescence intensity decay, the radiative (k_f) and radiationless (k_{nr}) rate constants can be calculated from the measured fluorescence quantum yield (φ_F) and fluorescence lifetime (τ) according to eqn:

$$k_f = \varphi_F/\tau \quad (17)$$

and

$$k_{nr} = (1 - \varphi_F)/\tau \quad (18)$$

Analysis of the influence of the solvent on the radiative and non-radiative rate constants gives information which of them depends on the solvent parameters enabling us to estimate which path of the excited state deactivation predominates. Moreover, the radiationless rate constant is the sum of the rate constant for internal conversion (k_{IC}) and rate constant for intersystem crossing (k_{ISC}). The value of the first one depends on the energy gap between the ground and excited states. If it correlates with the solvent polarity it indicates that the energy gap between these states decreases. In the opposite case, the main path of the excited state deactivation is intersystem crossing to the triplet state.

The multi-linear analysis of k_{nr} according to eqn (4) for **1** revealed that it does not correlate with solvent parameters (Table 4) in contrast to k_f which depends mainly on solvent dipolarity. A linear fit of k_{nr} *versus* ($\tilde{\nu}_{fluo}$) gives r = 0.1620, which means that the non-radiative rate constant probably does not depend on the energy gap between the ground and excited states. Moreover, this lack of correlation may indicate that the intersystem crossing is the main radiationless deactivation pathway and the excited state deactivation proceeds through the triplet state. A mean value of k_{nr} is equal to 1.5 ± 0.8 × 10^8 s^{-1}. As both k_f and ($\tilde{\nu}_{fluo}$) are controlled mainly by solvent dipolarity one can expect a linear dependence of k_f *versus* ($\tilde{\nu}_{fluo}$). Indeed, a linear dependence of $k_f = k_f^0 + \alpha(\tilde{\nu}_{fluo})$ is satisfactory (r = 0.9411). Thus, the invariance of k_{nr} and dependence of k_f on the solvent properties indicate that the change of the fluorescence quantum yield and the fluorescence decay time with solvent properties is mainly due to the change of the k_f rate constant.

A more complicated situation occurs for **2**. A multi-linear correlation according to eqn (4) reveals that there is no clear correlation between k_{nr} and Catalán solvent parameters (SP, SdP, SA, SB) taking into account the low value of r. Moreover, the fit with all four solvent parameters gives a little better r value (0.6696) than that with only solvent polarizability and acidity (r = 0.6349). The linear fit of k_{nr} *versus* ($\tilde{\nu}_{fluo}$) gives r = 0.5114 meaning that only 25% of k_{nr} changes results from the changes of the energy gap between the ground and excited states caused by increasing solvent polarity while the rest of the changes are determined by other factors. The multi-linear analysis of k_f according to eqn (4) gives a little better fit (r = 0.7129). The radiative rate constant depends on solvent properties in about 50% and all Catalán solvent parameters (SP, SdP, SA, SB) have impact on it. The mean value of k_f = 5.0 × 10^8 s^{-1} is one order higher than k_{nr} = 6 × 10^7 s^{-1} explaining high values of the fluorescence quantum yield of **2**.

According to Birks,[48] the radiative rate constant k_f divided by the square of the refractive index of a medium and average wavenumber of fluorescence in the third power is proportional to the squared transition dipole moment:

$$\frac{k_f}{n^2\tilde{\nu}_{fluo}^3} = \frac{16\pi^3}{3\varepsilon_0 h}\langle \Psi_G|\hat{\mu}|\Psi_E\rangle^2 \quad (19)$$

where $\hat{\mu}$ stands for the dipole moment operator, n is the refractive index of the medium, h is Planck's constant and ε_0 denotes the permittivity of vacuum. The multi-linear Catalán fit of $y = k_f/(n^2\tilde{\nu}_{fluo}^3)$ according to eqn (4) gives the information about the influence of solvent parameters on the transition dipole moment. For **2**, a low value of r = 0.7129 indicates that there is no clear correlation between $k_f/(n^2\tilde{\nu}_{fluo}^3)$ and the Catalán solvent parameters (SP, SdP, SA and SB) (Table 5). The lack of such a correlation was also established by Filarowski *et al.*[47] for BODIPY derivatives. The average value of $k_f/(n^2\tilde{\nu}_{fluo}^3)$ for the set of 33 solvents presented in Table 2 is 1.4 ± 0.6 × 10^{-5} s^{-1} cm^3. However, for **1** there is a clear correlation between $k_f/(n^2\tilde{\nu}_{fluo}^3)$ and the Catalán solvent parameters (r = 0.9160, Table 4). More detailed analysis shows that the solvent dipolarity is a major factor influencing the square of the transition dipole moment as derived from the linear fit of $k_f/(n^2\tilde{\nu}_{fluo}^3)$ as a function of SdP giving an r-value equal to 0.9054, just a little smaller than the original fit (0.9160).

3.3 Quantum chemical calculations

Theoretical calculations performed show that both compounds studied are not flat in the ground state as well as in the excited state. For compound **1**, the 2-phenyl-benzoxazole subunit forms a flat structure, whereas the carbazole moiety is twisted against the rest of the molecule. The dihedral angle is equal to 52.6° and 52.0° in acetonitrile (ε = 37.5) and cyclohexane (ε = 2), respectively. It is bigger than that for *N*-phenylcarbazole obtained from a semi-empirical calculation (AM1 method, 37.6 degrees[43]), but a little lower than that obtained at the DFT-B3LYP/6-311G(d,p) level (*ca.* 60°[13]). In the excited state, the carbazole subunit is oriented perpendicularly to the 2-phenyl-benzoxazole unit regardless of the solvent polarity.

A similar situation exists for **2**, but in this case a flat system is formed by benzoxazole and carbazole subunits whereas the phenyl ring forms with carbazole a dihedral angle equal to 57.7° in both solvents. In the excited state this dihedral angle decreases to 45.6° and 44.3° in cyclohexane and acetonitrile, respectively.

Applying the TD DFT method and the COSMO module the vertical absorption transitions for both compounds were calculated and are presented in the graphic form in Fig. 4 where vertical lines whose height is proportional to the oscillator strength and the theoretical absorption spectra have been simulated by considering a constant FWHM of 4000 cm^{-1}. Furthermore, in Fig. 4 experimental absorption spectra measured in cyclohexane and acetonitrile are also presented. Additionally, all calculated transitions with the oscillator strength higher than 0.1 and the molecular orbital contribution to the transition are collected in Tables 7S and 8S (ESI)† for **1** and **2**, respectively. Generally, the shape of theoretical absorption spectra calculated using the pbe0 functional reproduced the experimental spectra.

For **1**, both calculated spectra are a little red-shifted in the long-wavelength part, compared to the experimental ones, whereas the short-wavelength part of these spectra is very well reproduced. The long-wavelength absorption transition of **1** is mainly the HOMO → LUMO transition (contribution more than 98%, Table 7S (ESI)†). The HOMO has a pronounced π

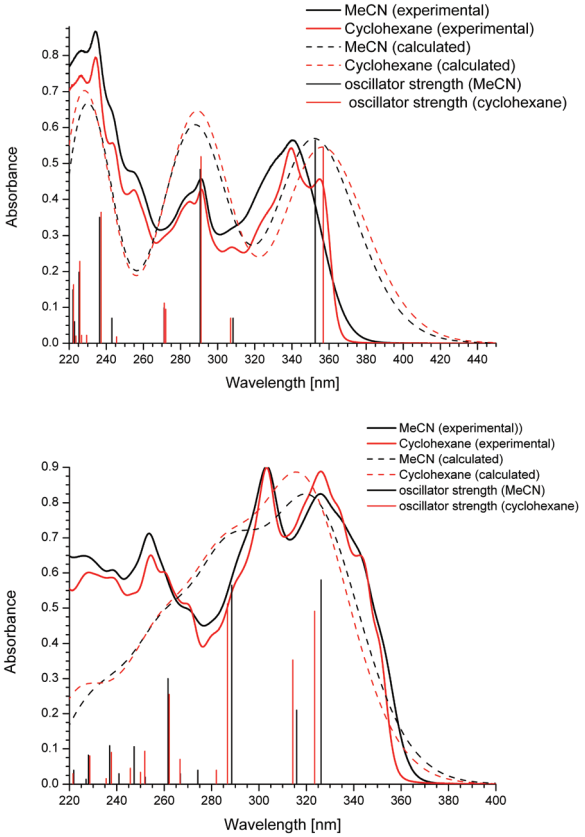

Fig. 4 Experimental and theoretically calculated absorption spectra as well as the oscillator strengths of calculated vertical transitions of **1** (at the top) and **2** (at the bottom) in MeCN and cyclohexane.

character localized on the carbazole moiety, whereas the LUMO has antibonding π character localized on the 2-phenylbenzoxazole moiety (Fig. 3S, ESI†). Thus, the HOMO → LUMO transition has an intramolecular charge-transfer character (Fig. 3S, ESI†). Contrary to the vertical absorption transition, the calculated vertical emission transition does not correctly reproduce the position of the emission spectrum of **1** in both studied solvents. The transition obtained from the calculation using the pbe0 functional is blue-shifted in acetonitrile compared to the experimental spectrum (λ_{cal} = 403.4 nm, λ_{max} = 447 nm), whereas it is red-shifted in cyclohexane (λ_{cal} = 401.4 nm, λ_{max} = 362 nm).

The difference in electron density between the ground and excited states of **1** shows that the emission transition possesses ICT character (HOMO–LUMO 98.5%) which generates a big excited state dipole moment (μ_{S1cal} = 19.7 D) – much bigger than that calculated based on the solvatochromic shift (μ_{S1} = 8.7 D, Table 3). The difference between wavelengths of calculated vertical emission transitions in acetonitrile and cyclohexane is due to the destabilization of the ground and excited states of **1** in cyclohexane compared to acetonitrile. The ground and excited state energies in cyclohexane are higher for about 42.6 kJ mol^{-1} and 26.5 kJ mol^{-1}, respectively, compared to acetonitrile. Moreover, for both solvents the character of the transition is the same (ICT) and the calculated excited state dipole moments are comparable (19.9 D in cyclohexane). The calculated oscillator strengths of emission transition are small (0.15 × 10^{-3} in acetonitrile (ε = 37.5) and 0.36 × 10^{-4} in cyclohexane (ε = 2)), which is consistent with the transition of ICT type but does not agree with large fluorescence quantum yield measured for **1** in acetonitrile (0.46) and cyclohexane (0.52).

In contrast to the geometrical parameters, which varied only slightly when different functionals are used, the excitation energies and theoretical oscillator strengths are sensitive to the choice of the functional. A crucial step in the theoretical investigations employing TD DFT is the choice of an approximate exchange–correlation functional and a reasonable basis set. Since one cannot expect that one approximate functional describes excited states of a molecule equally well, especially when different kinds of transitions are present (π → π* and CT).[49] It is well-known that for a large extended π system,[50] CT transitions are improperly reproduced by DFT calculations.[51] However, in such cases the pbe0 functional as well as BNL or CAM-B3LYP are recommended.[52]

For compound **2**, the first vertical absorption transition at 326.2 nm in acetonitrile (HOMO → LUMO, 85.4% and HOMO → LUMO + 1, 8.2%) agrees well with the experimental spectrum, however, the second transition at 315.9 nm (HOMO → LUMO + 1, 71.5%, HOMO − 2 → LUMO, 14.8%, HOMO → LUMO, 8.5%) is red-shifted, while the third at 288.5 nm (HOMO − 2 → LUMO, 71.7%, HOMO − 2 → LUMO + 1, 10.5%, HOMO → LUMO + 1, 9.0%) is blue-shifted according to the experimental spectrum (Fig. 4). Calculated absorption transitions, except for the first two absorption transitions, have small oscillator strengths compared to the experimental spectrum. The calculated vertical absorption transitions in cyclohexane, except being blue-shifted for a few nanometers, look very similar to those calculated for acetonitrile (Fig. 4, Table 8S, ESI†). One of the reasons which can explain to some extent the differences between theoretical and experimental oscillator strengths might be the intensity borrowing phenomena. The analysis of HOMO and LUMO orbitals of **2** (Fig. 4S, ESI†) reveals that contrary to **1** long-wavelength absorption transition has a π → π* character.

The optimized structure of **2** in the excited state is similar to the structure in the ground state. The subunit formed by benzoxazole and carbazole is flat, while the phenyl substituent is twisted. The dihedral angle between carbazole and phenyl rings decreased to about 45.6° in cyclohexane and 44.3° in acetonitrile. In both solvents the vertical emission transition occurs exclusively between LUMO and HOMO orbitals (95.9% in both solvents). The calculated emission transitions for **2** are blue-shifted for about 20 nm in both solvents, compared to the maxima of experimental emission spectra (ε = 2, λ_{cal} = 357 nm, λ_{max} = 374 nm; ε = 37.5, λ_{cal} = 361 nm, λ_{max} = 382 nm). Moreover, the calculated oscillator strength in cyclohexane is equal to f = 1.035, while for acetonitrile f = 0.915, which agrees well with large fluorescence quantum yields measured for that compound (0.76 and 0.99 in cyclohexane and acetonitrile, respectively). The electron density difference between the

ground and the excited state indicates a small charge transfer, which is reflected in the relatively small dipole moment of **2** in the excited state (5.95 D in cyclohexane and 9.45 D in acetonitrile, respectively). The excited state dipole moments of **2** are much smaller than those calculated for **1**. However, the value calculated for $\varepsilon = 37.5$ (acetonitrile) is far higher than the value determined from solvatochromic measurements (Table 3), while for $\varepsilon = 2$ (cyclohexane) they are comparable.

Theoretical calculations give information not only about dipole moments but also about the transition dipole moments and their relative orientation. The values of angles between absorption and fluorescence transition dipole moments obtained from theoretical calculations are equal to 0.3° for **1** and 4.1° for **2** (Fig. 5S and 6S, ESI†) whereas those obtained experimentally from fluorescence anisotropy measurements for stretched samples in PVA films are about 16.8° and 21°, respectively (Fig. 7S and 8S, ESI†). The experimental values do not fit very well to the Kawski–Gryczyński model, especially in the case of **2**, and should be treated only as approximate values. For compound **2** larger scatter of the experimental points is observed than for compound **1** which probably results from the differences in shapes of those compounds. The rotational ellipsoid of compound **1** is more elongated than that of compound **2**. Thus, compound **2** does not arrange appropriately along the stretching direction. The observed discrepancy between theoretical and experimental values may be a result of different environments used in each method (model of continuous solvent in theoretical calculations and PVA matrix in anisotropy measurements) as well as not appropriate model used for the calculation of the angle between transition dipole moments. However, both methods, experimental and theoretical, give higher values of that angle for compound **2**.

4 Conclusions

The analysis of photophysical properties of the compounds studied revealed that they are determined by the place of the *N*-phenylcarbazole substitution by the benzoxazole moiety. Introduction of carbazole in position 4 of the phenyl ring (compound **1**) leads to a compound with ICT type excited state with perpendicular orientation of the carbazole subunit in relation to a flat phenylbenzoxazole subunit. This in turn leads to a large excited state dipole moment and a large Stokes shift, similarly as in the case of 3-[2-(4-diphenylaminophenyl)benzoxazol-5-yl]alanine – the analogue without stiffening.[9] For this compound, the conformational freedom of phenyl substituents on the nitrogen atom as well as different coupling of non-bonding lone pair of the nitrogen atom with aromatic parts of the molecule suggest that the excited state dipole moment is higher. Moreover, in this case the influence of the character of the solvent is more pronounced.

A substitution in position 3 of the carbazole core leads to the compound with a little higher ground state dipole moment, however, with much smaller charge redistribution in the excited state in comparison to compound **1**. As a consequence, a smaller excited state dipole moment is observed for **2** which leads to the smaller Stokes shift. The different types of transitions ($\pi \rightarrow \pi^*$ for **2** and ICT for **1**) result in a higher fluorescence quantum yield observed for **2** than for **1**. The diverse charge distribution in the excited state of each compound suggests that the primary determinant of the photophysical properties in the multi-linear analysis is dipolarity for **1**, whereas for **2** – polarizability and dipolarity. Moreover, as both compounds contain a heterocyclic nitrogen atom some influence of solvent basicity and acidity is also recorded. As stated in the literature,[12,47] also this case revealed the predominance of a four-parameter solvent scale over three-parametric ones. A four-parameter solvent scale allows a deeper interpretation of the results due to the breakdown of the solvent polarizability/dipolarity parameter (π^* in the Kamlet–Taft scale or SPP in the old Catalán scale) into two new parameters – solvent polarizability (SP) and dipolarity (SdP).

The results of theoretical calculation significantly differ from experimental results, especially in the case of excited state dipole moment values and the influence of solvent polarity on the position of vertical transition. These discrepancies are connected with the simulation of the solvent polarity (COSMO model) used in the calculations which does not take into account specific solute–solvent interactions. However, the main reason is the method used (DFT) which for compounds as those described here with large extended π systems and/or exhibited charge transfer does not reproduce well experimental absorption and emission spectra in contrast to the geometrical parameters. The calculated geometries of the compounds studied in the ground and excited states help to explain the experimental results of solvatochromic studies (the character of the ground and excited states as well as the photophysical properties).

Both studied compounds show solvatochromism but their practical application may be limited as their spectral properties are in the UV range. However, changes in the carbazole substituent such as introduction of the electron-donating groups or extension of the aromatic ring will probably help to overcome this limitation by shifting the spectra of such derivatives bathochromically. Another possibility is alkylation of the benzoxazole nitrogen which not only changes the spectral properties of the compound but also should significantly improve its solubility in water.

Acknowledgements

This work was supported by the Polish Ministry of Science and Higher Education under grant DS-8441-4-0132-12.

Notes and references

1 J. R. Lakowicz, *Principles of Fluorescence Spectroscopy*, Kluwer Academic/Plenum Publishers, New York, 2nd edn, 1999.

2 M. R. Eftink and C. A. Ghiron, Exposure of tryptophanyl residues in proteins. Quantitative determination by fluorescence quenching studies, *Biochemistry*, 1976, **15**, 672–680.
3 J. R. Lombardi, Solvatochromic shifts reconsidered: field-induced mixing in the nonlinear region and application to indole, *J. Phys. Chem. A*, 1999, **103**, 6335–6338.
4 K. Guzow, M. Szabelski, J. Malicka and W. Wiczk, Synthesis of a new, highly fluorescent amino acid derivative: *N*-[(*tert*-butoxy)carbonyl]-3-[2-(1*H*-indol-3-yl)benzoxazol-5-yl]-L-alanine methyl ester, *Helv. Chim. Acta*, 2001, **84**, 1086–1092.
5 A. Rzeska, J. Malicka, K. Guzow, M. Szabelski and W. Wiczk, New highly fluorescent amino-acid derivatives: substituted 3-[2-(phenyl)benzoxazol-5-yl]-alanines: synthesis and photophysical properties, *J. Photochem. Photobiol., A*, 2001, **146**, 9–18.
6 K. Guzow, M. Szabelski, J. Malicka, J. Karolczak and W. Wiczk, Synthesis and photophysical properties of 3-[2-(pyridyl)benzoxazol-5-yl]-L-alanine derivatives, *Tetrahedron*, 2002, **58**, 2201–2209.
7 K. Guzow, K. Mazurkiewicz, M. Szabelski, R. Ganzynkowicz, J. Karolczak and W. Wiczk, Influence of an aromatic substituent in position 2 on photophysical properties of benzoxazol-5-yl-alanine derivatives, *Chem. Phys.*, 2003, **295**, 119–130.
8 K. Guzow, M. Szabelski, J. Karolczak and W. Wiczk, Solvatochromism of 3-[2-(aryl)benzoxazol-5-yl]alanine derivatives, *J. Photochem. Photobiol., A*, 2005, **170**, 215–223.
9 K. Guzow, M. Milewska and W. Wiczk, Solvatochromism of 3-[2-(4-diphenylaminophenyl)benzoxazol-5-yl]alanine methyl ester. A new fluorescence probe, *Spectrochim. Acta, Part A*, 2005, **61**, 1133–1140.
10 K. Guzow, J. Zielińska, K. Mazurkiewicz, J. Karolczak and W. Wiczk, Influence of substituents in the phenyl ring on photophysical properties of 3-[2-(phenyl)benzoxazol-5-yl]-alanine derivatives, *J. Photochem. Photobiol., A*, 2005, **175**, 57–68.
11 K. Guzow, D. Szmigiel, D. Wróblewski, M. Milewska, J. Karolczak and W. Wiczk, New fluorescence probes based on 3-(2-benzoxazol-5-yl)alanine skeleton – synthesis and photophysical properties, *J. Photochem. Photobiol., A*, 2007, **187**, 87–96.
12 K. Guzow, A. Ceszlak, M. Kozarzewska and W. Wiczk, Influence of substituents on the nitrogen atom of 3-[2-(4-aminophenyl)benzoxazol-5-yl]alanine derivatives on their photophysical properties – solvatochromic studies, *Photochem. Photobiol. Sci.*, 2011, **10**, 1610–1621.
13 O. Kwon, S. Barlow, S. A. Odom, L. Beverina, N. J. Thompson, E. Zojer, J.-L. Bredas and S. R. Marder, Aromatic amines: a comparison of electron-donor strengths, *J. Phys. Chem. A*, 2005, **109**, 9346–9352.
14 V. Perciuraite, S. Grigalevicius, J. Simokaitiene and J. V. Grazulevicius, Indolyl-substituted carbazole derivatives as amorphous electroactive materials for optoelectronics, *J. Photochem. Photobiol., A*, 2006, **182**, 38–42.
15 D. Kim, J. K. Lee, S. O. Kang and J. Ko, Molecular engineering of organic dyes containing *N*-aryl carbazole moiety for solar cell, *Tetrahedron*, 2007, **63**, 1913–1922.
16 C. Ito, M. Itoigawa, A. Sato, C. M. Hasan, M. A. Rashid, H. Tokuda, T. Mukainaka, H. Nishino and H. Furukawa, Chemical constituents of *Glycosmis arborea*: three new carbazole alkaloids and their biological activity, *J. Nat. Prod.*, 2004, **67**, 1488–1491.
17 Y. Liu, M. Nishiura, Y. Wang and Z. Hou, π-Conjugated aromatic enynes as a single-emitting component for white electroluminescence, *J. Am. Chem. Soc.*, 2006, **128**, 5592–5593.
18 M. V. Skorobogatyi, A. A. Pchelintseva, A. L. Petrunina, I. A. Stepanova, V. L. Andronova, G. A. Galegov, A. D. Malakhov and V. A. Korshun, 5-Alkynyl-2′-deoxyuridines, containing bulky aryl groups: evaluation of structure-anti-HIV-1 activity relationship, *Tetrahedron*, 2006, **62**, 1279–1287.
19 A. A. Kubicki, P. Bojarski, M. Grinberg, M. Sadownik and B. Kukliński, Time-resolved streak camera system with solid state laser and optical parametric generator in different spectroscopic applications, *Opt. Commun.*, 2006, **263**, 275–280.
20 M. J. Kamlet, J. L. M. Abbound and R. W. Taft, An examination of linear solvation energy relationships, *Prog. Phys. Org. Chem.*, 1982, **13**, 485–623.
21 M. J. Kamlet and R. W. Taft, Solvatochromic comparison method. 1. β-Scale of solvent hydrogen-bond acceptor (HBA) basicities, *J. Am. Chem. Soc.*, 1976, **98**, 377–383.
22 R. W. Taft and M. J. Kamlet, Solvatochromic comparison method. 2. α-Scale of solvent hydrogen-bond donor (HBD) acidities, *J. Am. Chem. Soc.*, 1976, **98**, 2886–2894.
23 M. J. Kamlet, J. L. M. Abboud and R. W. Taft, Solvatochromic comparison method. 6. π* Scale of solvent polarities, *J. Am. Chem. Soc.*, 1977, **99**, 6027–6038.
24 J. Catalán, V. López, P. Pérez, R. Martin-Villamil and J. G. Rodriguez, Progress towards a generalized solvent polarity scale – The solvatochromism of 2-(dimethylamino)-7-nitrofluorene and its homophorm 2-fluoro-7-nitrofluorene, *Liebigs Ann.*, 1995, 241–252.
25 J. Catalán and C. Díaz, A generalized solvent acidity scale: the solvatochromism of *o*-*tert*-butylstilbazolium betaine dye and its homophorm *o*,*o*′-di-*tert*-butylstilbazolium betaine dye, *Liebigs Ann. Recl.*, 1997, 1941–1949.
26 J. Catalán, C. Díaz, V. López, P. Pérez, J. L. G. de Paz and J. G. Rodriguez, A generalized solvent basicity scale: the solvatochromism of 5-nitroindoline and its homophorm 1-methyl-5-nitroindoline, *Liebigs Ann.*, 1996, 1785–1794.
27 J. Catalan and H. Hopf, Empirical treatment of the inductive and dispersive component of solute-solvent interactions: the solvent polarizability (SP) scale, *Eur. J. Org. Chem.*, 2004, 4694–4702.
28 J. Catalán, Toward a generalized treatment of the solvent effect based on four empirical scales: dipolarity (SdP, a new scale), polarizability (SP), acidity (SA), and basicity (SB) of the medium, *J. Phys. Chem. B*, 2009, **113**, 5951–5960.

29 A. Kawski, in *Progress in Photochemistry and Photophysics*, ed. J. F. Rabek, CRC Press, Boca Raton, USA, 1992, vol. 5.
30 A. Kawski and P. Bojarski, in *Chromic Materials, Phenomena and their Technological Applications*, ed. P. R. Somani, Applied Science Innovations, 2009.
31 A. Kawski, B. Kukliński and P. Bojarski, Dipole moment of aniline in the excited S_1 state from thermochromic effect on electronic spectra, *Chem. Phys. Lett.*, 2005, **415**, 251–255.
32 A. Kawski, Ground- and excited-state dipole moments of 6-propionyl-2-(dimethylamino)naphthalene determined from solvatochromic shifts, *Z. Naturforsch.*, 1999, **54a**, 379–381.
33 A. Kawski and Z. Gryczyński, On the determination of transition-moment directions from emission anisotropy measurements, *Z. Naturforsch.*, 1986, **41a**, 1195–1199.
34 A. Kawski and Z. Gryczyński, Determination of the transition-moment directions from photoselection in partially oriented systems, *Z. Naturforsch.*, 1987, **42a**, 808–812.
35 Z. Gryczyński and A. Kawski, Relation between the emission anisotropy and the dichroic ratio for solute alignment on stretched polymer films, *Z. Naturforsch.*, 1987, **42a**, 1396–1398.
36 Z. Gryczyński and A. Kawski, Directions of the electronic transition moments of dioxydo-*p*-terphenyl, *Z. Naturforsch.*, 1988, **43a**, 193–195.
37 A. Synak and P. Bojarski, Transition moment directions of selected carbocyanines from emission anisotropy and linear dichroism measurements in unaxially stretched polymer films, *Chem. Phys. Lett.*, 2005, **416**, 300–304.
38 J. Michl and E. W. Thulstrup, *Spectroscopy with Polarized Light*, VCH Publ. Inc., New York, 1986.
39 Y. Tanizaki, T. Kobayashi and N. Ando, The relation between the deformation of substrate of PVA sheet by stretching and the stretch ratio-RS, *Bull. Chem. Soc. Jpn.*, 1959, **32**, 1362–1363.
40 Y. Tanizaki, Correction of relation of optical density ratio to stretch ratio on dichroic spectra, *Bull. Chem. Soc. Jpn.*, 1965, **38**, 1798–1799.
41 http://avogadro.openmolecules.net/
42 A. Sarkar and S. Chakravorti, A solvent-dependent luminescence study on 9-phenylcarbazole, *J. Lumin.*, 1998, **78**, 205–211.
43 S. M. Bonesi and R. Erra-Balsells, Electronic spectroscopy of carbazole and N- and C-substituted carbazoles in homogeneous media and in solid matrix, *J. Lumin.*, 2001, **93**, 51–74.
44 G. E. Johnson, Fluorescence quenching of carbazoles, *J. Phys. Chem.*, 1980, **84**, 2940–2946.
45 M. Ravi, A. Samanta and T. P. Radhakrishnan, Excited state dipole moments from an efficient analysis of solvatochromic stokes shift data, *J. Phys. Chem.*, 1994, **98**, 9133–9136.
46 S. Kumar, V. C. Rao and R. C. Rostogi, Excited-state dipole moments of some hydroxycoumarin dyes using an efficient solvatochromic method based on the solvent polarity parameter, E_T^N, *Spectrochim. Acta, Part A*, 2001, **57**, 41–47.
47 A. Filarowski, M. Kluba, K. Cieślik-Boczula, A. Koll, A. Kochel, L. Pandey, W. M. de Borggewaeve, M. van der Auweraer, J. Catalán and N. Boens, Generalized solvent scales as a tool for investigating solvent dependence of spectroscopic and kinetic parameters. Application to fluorescent BODIPY dyes, *Photochem. Photobiol. Sci.*, 2010, **9**, 996–1008.
48 J. B. Birks, *Photophysics of Aromatic Molecules*, Wiley-Interscience, London, 1970.
49 A. Dreuw and M. Head-Gordon, Single-reference ab initio methods for the calcualtion of excited states of large molecules, *Chem. Rev.*, 2005, **105**, 4009–4037.
50 Z.-L. Cai, K. Sendt and J. R. Reamers, Failure of density-functional theory and time-dependent density-functional theory for large extended π systems, *J. Chem. Phys.*, 2002, **117**, 5543–5549.
51 A. Dreuw and M. Head-Gordon, Failure of time-dependent density functional theory for long-range charge-transfer excited states: the zincbacteriochlorin-bacteriochlorin and bacteriochlorophyll-spheroidene complexes, *J. Am. Chem. Soc.*, 2004, **126**, 4007–4016.
52 J. Andzelm, B. C. Rinderspacher, A. Rawlett, J. Dougherty, R. Baer and N. Govind, Performance of DFT methods in the calculation of optical spectra of TCF-chromophores, *J. Chem. Theor. Comput.*, 2009, **5**, 2835–2846.